The impact of aging and gender on brain viscoelasticity ☆

Ingolf Sack [a],[*], Bernd Beierbach [a], Jens Wuerfel [b], Dieter Klatt [a], Uwe Hamhaber [c], Sebastian Papazoglou [a], Peter Martus [d], Jürgen Braun [c]

[a] Department of Radiology, Charité — University Medicine Berlin, Campus Charité Mitte, Berlin, Germany
[b] Institute of Neuroradiology, University Schleswig-Holstein, Campus Luebeck, Germany
[c] Institute of Medical Informatics, Charité — University Medicine Berlin, Campus Benjamin Franklin, Berlin, Germany
[d] Institute of Biometry and Clinical Epidemiology, Charité — University Medicine Berlin, Campus Benjamin Franklin, Berlin, Germany

ARTICLE INFO

ABSTRACT

Viscoelasticity is a sensitive measure of the microstructural constitution of soft biological tissue and is increasingly used as a diagnostic marker, e.g. in staging liver fibrosis or characterizing breast tumors. In this study, multifrequency magnetic resonance elastography was used to investigate the in vivo viscoelasticity of healthy human brain in 55 volunteers (23 females) ranging in age from 18 to 88 years. The application of four vibration frequencies in an acoustic range from 25 to 62.5 Hz revealed for the first time how physiological aging changes the global viscosity and elasticity of the brain. Using the rheological springpot model, viscosity and elasticity are combined in a parameter μ that describes the solid-fluid behavior of the tissue and a parameter α related to the tissue's microstructure. It is shown that the healthy adult brain undergoes steady parenchymal 'liquefaction' characterized by a continuous decline in μ of 0.8% per year ($P<0.001$), whereas α remains unchanged. Furthermore, significant sex differences were found with female brains being on average 9% more solid-like than their male counterparts rendering women more than a decade 'younger' than men with respect to brain mechanics ($P=0.016$). These results set the background for using cerebral multifrequency elastography in diagnosing subtle neurodegenerative processes not detectable by other diagnostic methods.

© 2009 Elsevier Inc. All rights reserved.

Introduction

Physiological aging of the brain is accompanied by ubiquitous degeneration of neurons and oligodendrocytes (Morrison and Hof, 1997). An alteration of the cellular matrix of an organ impacts its macroscopic viscoelastic properties, which are characterized by mechanical parameters such as stiffness and internal friction (Fung, 1993). These properties are intuitively exploited during palpation, which assesses the stiffness of soft tissue to 'feel' structural changes associated with disease. Until recently, the measurement of viscoelastic properties of the brain required an intervention (Hrapko et al., 2008), which is why there is a lack of knowledge about the mechanical behavior of the healthy brain in its intact physiological environment. To date almost nothing is known about alterations of in vivo cerebral viscoelasticity associated with diffuse structural changes during normal aging (Thibault and Margulies, 1998). Although conventional magnetic resonance imaging (MRI) has become the most important neuroimaging modality, its capability to identify diffuse structural changes of the brain parenchyma is limited (Mueller et al., 2006).

Combining MRI with acoustic waves is a new and promising way to measure cerebral viscoelasticity without intervention (McCracken et al., 2005). Recently, the technical feasibility of brain MR elastography was demonstrated; however, different and partially contradicting results were reported (Hamhaber et al., 2007; Klatt et al., 2007; Vappou et al., 2007; Xu et al., 2007; Kruse et al., 2008; Sack et al., 2008; Green et al., 2008). The disparity of data may result from a well known phenomenon in material testing: the frequency dispersion of the material's inherent complex modulus. The real part of the complex modulus (G') is determined by the restoration of mechanical energy due to the elastic properties of the material, while its imaginary part (G'') is associated with loss of energy as a result of the mechanical friction inherent to the material. As former studies were conducted using single wave frequencies, the derived viscoelastic parameters are bound to specific experimental conditions and thus not generally valid. In contrast, multifrequency MRE is capable of measuring the dispersion of the complex modulus (G) in the target tissue, thereby improving the physical significance of MRE data by utilizing higher-order viscoelastic models (Klatt et al., 2007; Asbach et al., 2008). The purpose of this study was to set up a clinically applicable assay of multifrequency MRE of the brain and to measure cerebral viscoelasticity as a function of age and sex in 55 individuals. Our hypothesis was that the viscoelasticity of the brain is sensitive to a widespread structural alteration occurring in the course of physiological aging. It

has also been discussed that cerebral viscoelasticity may provide a sensitive marker for a variety of neurological diseases such as normal pressure hydrocephalus, Alzheimer's disease, or Multiple Sclerosis (Kruse et al., 2008; Wuerfel et al., 2008). Therefore, the results presented in this study are intended as background data for future applications of brain MRE in patients.

Materials and methods

This study was approved by the ethics committee of the Charité – University Medicine Berlin (directive EA1/182/07) and written informed consent was obtained from all subjects. Fifty-five volunteers without overt neurological or psychiatric conditions were recruited for this study (mean age 49.35 years, standard deviation [SD] 18.78 years, age range 18 to 88 years; 31 males, mean age 52.74 years, SD 17.61 years, age range 21 to 84 years; 24 females, mean age 44.96 years, SD 19.70 years, age range 18 to 88 years). Experiments were run on a standard 1.5 T clinical MRI scanner (Siemens, Erlangen, Germany). A custom-made head cradle shown in Fig. 1 was manually adjusted before each MRE examination to ensure that the subject's head was placed in the center of the MRI head coil about 3 to 5 cm away from the pivot. Multifrequency vibration as described in (Klatt et al., 2007) with a maximum amplitude of approximately 1 mm in parallel direction to the long axis of the magnet was fed into the actuator by a carbon fiber piston. The vibration was well tolerated by the volunteers, as reflected by the fact that only one subject felt uncomfortable during vibration, while all others described the stimulation as a negligible tingling.

Wave image acquisition was performed using a single-shot echo-planar imaging sequence, that was sensitized to vibration by a sinusoidal gradient of four periods and 60 Hz frequency (Klatt et al., 2007). Three transverse image slices with through-plane motion-encoding direction were selected in a central slab through the cerebrum. Acquisition was repeated 80 times for each image slice with an alternating sign of motion sensitization and an increasing delay between start of vibration and motion encoding. The resulting 40 time-resolved phase-difference wave images, $u(x, y, t)$ (with x and y as spatial coordinates), were Fourier-transformed for decomposition into complex wave images at driving frequency: $U(x, y, \omega)$, ($\omega/2\pi = 25$, 37.5, 50 and 62.5 Hz). Complex modulus images were obtained by planar wave inversion ($G(x, y, \omega) = -\rho\omega^2 U/\Delta U$, with Δ as the Laplace operator and ρ as the unit density of 1000 kg/m³) (Papazoglou et al., 2008). Fig. 2 shows the image data $U(x, y, \omega)$ and $G(x, y, \omega)$ of one volunteer. $G(x, y, \omega)$ was spatially averaged within brain parenchyma, displayed by three transverse image slices (excluding ventricles and cerebrospinal fluid). The resulting global

modulus function $G(\omega)$ was fitted by the springpot model (Koeller, 1984; Sinkus et al., 2007; Klatt et al., 2008)

$$G_{\mathrm{model}} = \kappa(i\omega)^{\alpha}. \tag{1}$$

κ and α were varied in a least-square fit routine for minimizing the variance

$$\chi^2 = \frac{1}{4}\sum_{n=2}^{5} (G'(\omega_n) - G'_{\mathrm{model}}(\omega_n))^2 + (G''(\omega_n) - G''_{\mathrm{model}}(\omega_n))^2. \tag{2}$$

The prime refers to the real part of the complex modulus (storage modulus), while the double prime denotes its imaginary part (loss modulus). ω_n is the angular drive frequency: $\omega_n = 2\pi$ 12.5 Hz n. Finally, κ was transformed to a parameter of the dimension of the shear modulus

$$\mu = (\kappa\eta^{-\alpha})^{\frac{1}{1-\alpha}} \tag{3}$$

assuming a viscosity parameter η of 3.7 Pa s (for further details see Fig. 3 and the Results and discussion section). Voigt, Maxwell and Zener fits were performed as described previously (Klatt et al., 2007; Asbach et al., 2008).

Statistical data analysis

Four storage moduli G', four loss moduli G'', and nine constitutive parameters according to Voigt, Maxwell, springpot, and Zener models were analyzed. All moduli G' and G'' as well as viscoelastic model parameters with the exception of the springpot-parameter α were highly correlated and showed comparable results. Therefore, no adjustment for multiple testing was applied. All data were distributed approximately normally. Linear regression models with age and sex as covariates were applied. Although the age effect seemed to be different for male and female subjects, the formal test of interaction was not significant, so that only a constant slope model was used. Differences between groups were transformed to the age scale by dividing the parameters of the group differences by the slope of age. The level of significance was 0.05 (two-sided); all analyses were carried out using SPSS for Windows (release 15.0).

Results and discussion

Fig. 2 presents wave data acquired in a central transverse image slice by multifrequency head stimulation. Complex wave images $U(x, y, \omega)$ convey the information about elastic material properties by wavelengths, while viscous properties are attainable from wave damping. Evaluation of the attenuation of the waves requires knowledge about the wave-propagation direction that is implicitly given by the phase shift between the real and the imaginary part of the waves. The appearance of wave patterns might vary considerably within one and the same volunteer, as it is influenced by the position of the head within the cradle, the exact slice location and the amplitude of the wave generator. However, as demonstrated in (Sack et al., 2008), wave inversion yields consistent and well reproducible values of elasticity and viscosity, if $G(x, y, \omega)$ is spatially averaged within larger areas of the brain. Given the relatively low resolution of the G' and G'' maps in Fig. 2, they may be more suited as a test of the overall status of the brain, as opposed to the detection of local pathology. Therefore, in this study no spatial variation but the increase of the averaged $G(x, y, \omega)$-intensity over drive frequency was analyzed. This dispersion is better represented by mean $G'(\omega)$ and $G''(\omega)$-dispersion functions as shown in Fig. 3 for two volunteers displaying a large age-disparity. The decrease of both storage and loss modulus due to senescence is immediately perceptible. Furthermore, this age-related decline
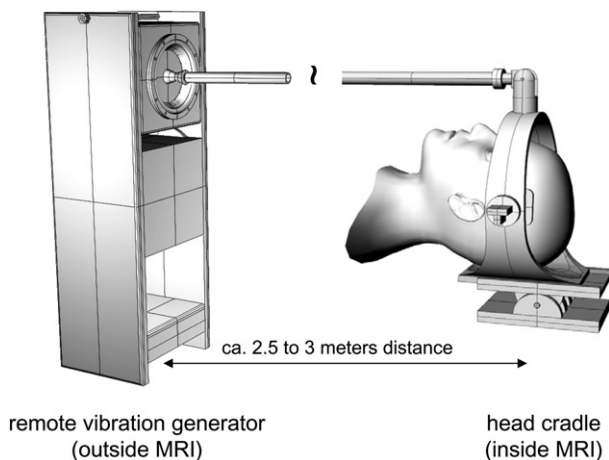

ca. 2.5 to 3 meters distance

remote vibration generator (outside MRI)

head cradle (inside MRI)

Fig. 1. Head actuator used for stimulating low-frequency shear vibrations in the brain.
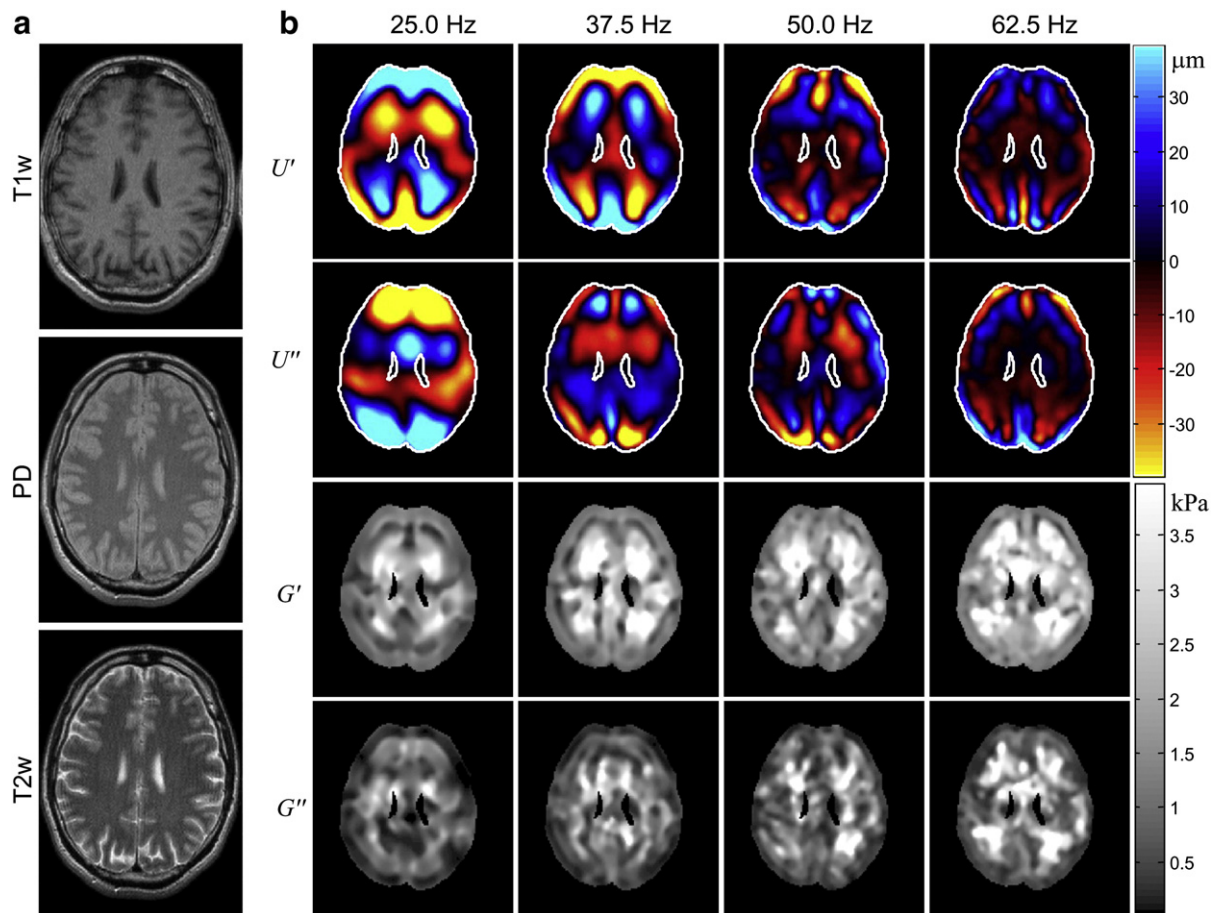
Fig. 2. Illustration of the outcome of a single-slice multifrequency-MRE experiment of a 47-year old male volunteer. (a) Standard MRI data as anatomical reference (T1w, PD, T2w: T1-weighted, proton density and T2-image contrast, respectively). (b) Wave images (U' and U'' denote real and imaginary part of $U(x, y, \omega)$) and complex modulus images (G' and G'' denote real and imaginary part of $G(x, y, \omega)$). Drive frequencies used in experiments ($\omega/2\pi$) are given above the columns. After spatial averaging with two other image slices, four complex moduli $G(\omega)$ per volunteer are obtained whose frequency dispersion was analyzed as demonstrated in Fig. 3.

appears to occur in the entire frequency range. This observation is supported by the relative decline of G' and G'' of all volunteers ranging from 0.4% (at 25 Hz) to 0.7% (at 62.5 Hz) for G', and from 0.6% (at 25 Hz) to 0.8% (at 62.5 Hz) for G'' (always $P<0.01$). The entire list of the mean complex moduli and their decay rates is given in Tables 1 and 2.

A generalized (frequency-independent) representation of viscoelasticity can be obtained by combining springs and dashpots as a model for energy storage (elasticity) and energy loss (viscosity) denoted by μ [Pa] and η [Pas] respectively (Tschoegl, 1989). In order to apply an adequate fitting paradigm, we focused on the following model characteristics:

- Physical significance: The stress-strain function of the model sustains causality (Tschoegl, 1989).
- Least number of free parameters: The experimental dispersion of G should be fitted by only two parameters.

These properties apply to three well known rheological models: The Maxwell-, the Voigt- and the springpot model, comprising a spring and a dashpot in serial circuitry, parallel alignment, and in the interpolative combination yielding the fractional element $\kappa = \mu^{1-\alpha}\eta^{\alpha}$, respectively (Tschoegl, 1989). In the fractional element model, a pure elastic solid is characterized by $\alpha=0$, whereas a viscous fluid without energy-restoration is of $\alpha=1$. Usually, soft biological tissue values are between these limits. Fig. 3 shows a comparison of models fitting the complex modulus data of two volunteers. It can be clearly seen that the increase in G'' with increasing frequency is well represented by Voigt's loss modulus, while G' dispersion is better described by the Maxwell model. However, the standard MRE approach employs the

Voigt model for fitting G', which is inappropriate in the light of multifrequency MRE. The best match between model and multifrequency data is achieved by a combination of Voigt and Maxwell models given by the Zener model. However, this model incorporates an additional parameter – a second shear modulus – rendering the interpretation of viscoelastic constants rather cumbersome. In this context it is worthwhile to mention that linear functions can fit G within the examined frequency range; however, then four independent parameters are required (two axis intercepts and two slopes). Furthermore the meaning of such arbitrary parameters is limited, as independent linear functions do not fulfill causality. A combined linear fit of G' and G'' is achieved by the springpot on a logarithmic scale, where α represents the slope of the complex modulus. Henceforth the springpot is considered our reference two-parameter model since it provides the best tradeoff between physical significance and representation of the frequency dependency of our data by only two parameters. As κ has a rather cumbersome dimension of $Pa^{(1-\alpha)}(Pas)^{\alpha}$ we transformed this mixed viscoelastic constant to a parameter related to shear elasticity μ taking $\eta=3.7$ Pa s as the mean viscosity of all volunteers according to the Zener model (see Table 1). Linear regression revealed a decrease in μ of 15 Pa per year (0.8%, $P<0.001$) in healthy brain, whereas α was nearly constant with 0.264 ± 0.01 and a slope of $(-15\pm7)\times10^{-5}$ (0.06%, $P<0.05$) (see Fig. 4 and Tables 1 and 2). The annual decline of the springpot-μ of 0.8% is the largest effect of aging revealed by a viscoelastic constant in our models. This high sensitivity of the springpot model to aging is further supported by the high R^2-value, presented in Table 2, which is only exceeded by R^2 of the viscosity parameter of the Voigt's model.
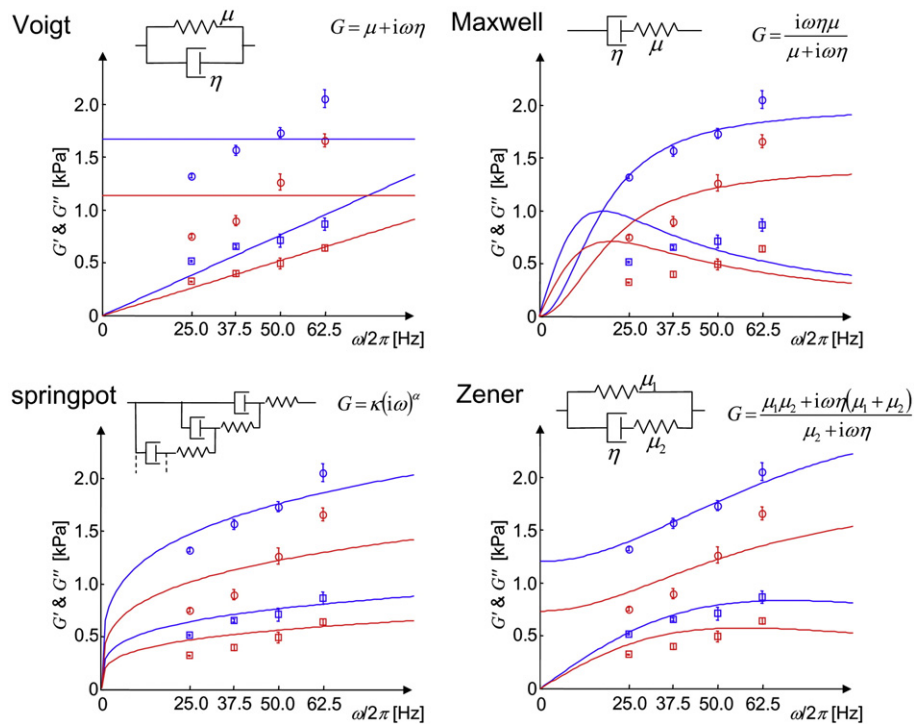
Fig. 3. Representations of the complex modulus $G(\omega)$ as real and imaginary parts on a frequency axis (storage and loss modulus G' and G'' are represented by circles and squares, respectively). Blue data correspond to the youngest volunteer (female, 18 years) while red data represent the oldest volunteer in our cohort (female, 88 years). Fits were performed according to the simplest (two-parameter) viscoelastic models and the Zener model. In addition, the spring-dashpot representations of all models together with the fit functions, $G(\omega)$, are given.

We further accounted for gender-related aspects of cerebral viscoelasticity. Clear sex differences were observed with female brains being in the order of 180 Pa (9%) stiffer than those of males ($P<0.05$). This difference can be translated into a scale of *viscoelastic age*, according to which female brains were on average 13 years ($P<0.05$) younger than male brains. The analysis of the sex differences of all moduli is presented in Table 3.

Elderly men and young women represented the minimum and the maximum in our range of brain viscoelasticities, respectively. Interestingly, this finding is not correlated to the volume of the adult brain, measured as brain parenchymal fraction, which is smallest in elderly females (Dekaban, 1978; Good et al., 2001). We therefore conclude that brain geometry and volume only have a minor influence on our data. This conclusion is supported by the aforementioned fact that the observed age dependency of the complex modulus G does not change with drive frequency. In contrast, wave reflections and diffractions at sites of tissue boundaries are highly frequency dependent (Papazoglou et al., 2008; Papazoglou et al., 2007). Thus, the decrease in the parenchyma/CSF ratio, which is accompanied by an increase in ventricle volume and sulcus size, would result in

Table 1
Description of the complex moduli G measured at four different drive frequencies.

	All subjects	Females	Males
Storage and loss moduli [kPa]			
G' (25 Hz)	1.11 (0.21)	1.18 (0.19)	1.04 (0.20)
G' (37.5 Hz)	1.31 (0.28)	1.42 (0.28)	1.22 (0.25)
G' (50 Hz)	1.52 (0.22)	1.60 (0.23)	1.45 (0.20)
G' (62.5 Hz)	2.01 (0.23)	2.10 (0.24)	1.95 (0.20)
G'' (25 Hz)	0.48 (0.10)	0.52 (0.10)	0.45 (0.10)
G'' (37.5 Hz)	0.57 (0.13)	0.62 (0.13)	0.53 (0.12)
G'' (50 Hz)	0.60 (0.11)	0.63 (0.11)	0.57 (0.10)
G'' (62.5 Hz)	0.80 (0.13)	0.85 (0.13)	0.76 (0.12)
Viscoelastic models			
Springpot (α)	0.264 (0.01)	0.265 (0.009)	0.263 (0.011)
Springpot (μ)[a]	1.94 (0.39)	2.10 (0.39)	1.81 (0.34)
Voigt (η)[b]	2.13 (0.36)	2.28 (0.35)	2.02 (0.33)
Voigt (μ)[a]	1.49 (0.22)	1.58 (0.22)	1.42 (0.2)
Maxwell (η)[b]	15.18 (2.55)	16.18 (2.53)	14.41 (2.31)
Maxwell (μ)[a]	1.80 (0.27)	1.91 (0.26)	1.71 (0.24)
Zener (η)[b]	3.85 (0.58)	4.06 (0.57)	3.70 (0.55)
Zener (μ_1)[a]	0.99 (0.16)	1.06 (0.16)	0.94 (0.13)
Zener (μ_2)[a]	1.46 (0.23)	1.55 (0.23)	1.38 (0.21)

The standard deviations (SD) of G and of the model parameters are given in brackets. Springpot, Voigt, Maxwell, and Zener refer to the respective models as plotted in Fig. 3.
[a] kPa.
[b] Pa s.

Table 2
Age dependencies of complex moduli and viscoelastic parameters.

Parameter X	R-square	Annual change in X	Annual change in X [%]	P-value
Storage and loss moduli				
G' (25 Hz)[a]	0.54	−8.2	−0.7	<0.001
G' (37.5 Hz)[a]	0.39	−9.4	−0.7	<0.001
G' (50 Hz)[a]	0.50	−8.4	−0.6	<0.001
G' (62.5 Hz)[a]	0.37	−7.5	−0.4	<0.001
G'' (25 Hz)[a]	0.52	−3.9	−0.8	<0.001
G'' (37.5 Hz)[a]	0.49	−4.9	−0.9	<0.001
G'' (50 Hz)[a]	0.46	−3.9	−0.7	<0.001
G'' (62.5 Hz)[a]	0.41	−4.4	−0.6	<0.001
Viscoelastic models				
Springpot (α)	0.08	0.000	−0.1	<0.05
Springpot (μ)[a]	0.52	−15.0	−0.8	<0.001
Voigt (η)[b]	0.55	−0.014	−0.7	<0.001
Voigt (μ)[a]	0.51	−8.4	−0.6	<0.001
Maxwell (η)[b]	0.44	−0.090	−0.6	<0.001
Maxwell (μ)[a]	0.52	−10.2	−0.6	<0.001
Zener (η)[b]	0.50	−0.022	−0.6	<0.001
Zener (μ_1)[a]	0.46	−5.7	−0.6	<0.001
Zener (μ_2)[a]	0.51	−8.8	−0.6	<0.001

The annual change is the slope of the regression line with dimension Pascal per year (for elastic moduli), Pascal second per year (for viscosity parameters) or one over year (for the structural parameter α).

[a] [Pa/year].
[b] [Pa s/year].

Table 3
Sex differences of complex moduli and viscoelastic model parameters according to a linear regression model with age and sex as predictors.

Parameter X	ΔX females vs males[a]	ΔX females vs males[a] [%]	Delay[b] [years]	P-value
Storage and loss moduli				
G' (25 Hz)[c]	0.080	7	10.0	0.041
G' (37.5 Hz)[c]	0.139	11	15.4	0.023
G' (50 Hz)[c]	0.090	6	11.3	0.039
G' (62.5 Hz)[c]	0.096	5	13.7	0.060
G'' (25 Hz)[c]	0.056	12	9.8	0.039
G'' (37.5 Hz)[c]	0.053	9	10.8	0.054
G'' (50 Hz)[c]	0.048	8	7.8	0.031
G'' (62.5 Hz)[c]	0.047	6	14.8	0.059
Viscoelastic models				
Springpot (α)	0.001	0	3.5	0.85
Springpot (μ)[c]	0.180	9	12.9	0.016
Voigt (η)[d]	0.156	7	12.0	0.020
Voigt (μ)[c]	0.101	7	12.6	0.018
Maxwell (η)[d]	1.117	7	13.3	0.035
Maxwell (μ)[c]	0.118	7	11.8	0.020
Zener (η)[d]	0.189	5	9.0	0.103
Zener (μ_1)[c]	0.079	8	15.8	0.013
Zener (μ_2)[c]	0.105	7	13.1	0.020

[a] ΔX females vs males refers to the difference of intercepts for both groups in the linear regression model with equal slope for males and females.
[b] The delay relates the difference between male and female subjects to the age interval during which identical losses occur (quotient of the sex difference ΔX and the annual change in X).
[c] [kPa].
[d] [Pa s].

different age effects at different driving frequencies. The fact that this was not observed in our data provides strong evidence that MRE is stable against effects related to tissue boundaries and interfaces.

Moreover, the observed age and sex effects were largely independent of the applied model. Indeed, all models investigated displayed an age-related decline in both elasticity and viscosity. The constant ratio of both properties was underscored by a widely constant and insignificant parameter α. This is of importance, since the ratio of elastic and viscous properties characterizes the *structure* of the tissue (corresponding to the hypothetical alignment of springs and dashpots), whereas the order of magnitude of viscoelastic parameters determines the solid-fluid behavior of the material. The latter was given in our springpot-μ, combining elastic and viscous information in the combined property of *viscoelasticity*. Assuming preservation of the geometry of the material's structure (i.e. α is constant), alterations in μ indicate a continuous phase transition on a solid-fluid scale. This tissue "liquefaction" raises the question of how neurons and glial cells may contribute to the global mechanical properties of the brain parenchyma. Glial cells were recently found to be "softer" than

neurons, contradicting the notion that glial cells provide a supporting mechanical scaffold for neurons (Lu et al., 2006).

Based on our observation, one can speculate about the neuropathological correlate of the liquefaction detected by MRE in the aging brain: Is this liquefaction a consequence of the "naturally" decreasing number or the size of neurons during lifetime (Pakkenberg et al., 2003; Hsu et al., 2008), leading to a relatively higher proportion of softer glial cells? This hypothesis is supported by reports of a decreasing neuron–glia ratio in healthily aging brains (Terry et al., 1987) and, consistent with the sex disparity observed by MRE, a higher neuron–glia ratio in women than in men (Pelvig et al., 2007). Clearly, this tentative interpretation does not account for more elaborate cellular force-feedback loops given by the active and nonlinear response of cells to a changing mechanical environment (Discher et al., 2005; Van Essen, 1997). Such nonlinear responses have been described for cytoskeletal rigidity, cell adhesion, and other cellular processes which may cause a viscoelastic "hyper-response" of
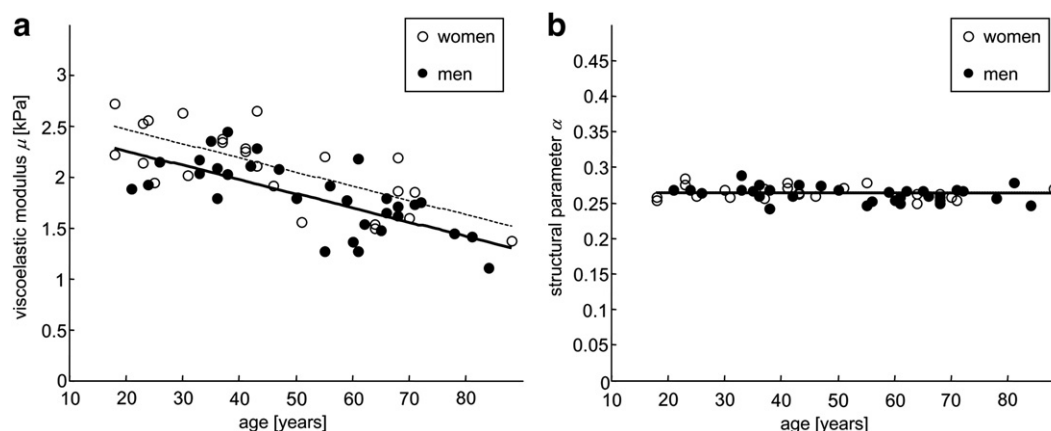

Fig. 4. (a) Brain viscoelasticity parameters according to the springpot model. μ represents both elastic (stiffness) and viscous (friction) properties of brain tissue and is thus a measure of adhesion and 'connectivity' of soft tissue cells. In contrast to μ, α does not significantly change with age and sex (b), indicating a relative constant geometrical alignment of structural building blocks in the healthy adult brain. Linear regression graphs were plotted separately for women (dotted line) and men (solid line).

the brain exceeding the effects measured by other quantitative MRI techniques (Mueller et al., 2006).

Irrespective of histopathological evidence supporting our results, viscoelastic properties might become a surrogate marker for the state of health of the brain parenchyma, similar to the clinical findings derived from the palpation of other organs. As brain MRE is only at the beginning of its technical development, it is expected that the method will become more accurate in the future. With further refinement, position-resolved viscoelastic constants may shed light on more specific mechanisms of aging with respect to different types of cerebral tissue and regions of the brain.

In summary, it was demonstrated that multifrequency MRE provides a sensitive measure of the global integrity of brain tissue. Using this new technique for the diagnosis of diffuse pathological processes, one needs to account for age- and sex-related effects on viscoelastic constants of the brain.

References

Asbach, P., Klatt, D., Hamhaber, U., Braun, J., Somasundaram, R., Hamm, B., Sack, I., 2008. Assessment of liver viscoelasticity using multifrequency MR elastography. Magn. Reson. Med. 60, 373–379.

Dekaban, A.S., 1978. Changes in brain weights during the span of human life: relation of brain weights to body heights and body weights. Ann. Neurol. 4 (4), 345–356.

Discher, D.E., Janmey, P., Wang, Y.L., 2005. Tissue cells feel and respond to the stiffness of their substrate. Science 310 (5751), 1139–1143.

Fung, Y., 1993. Biomechanics: Mechanical Properties of Living Tissue. Springer-Verlag, New York.

Good, C.D., Johnsrude, I.S., Ashburner, J., Henson, R.N., Friston, K.J., Frackowiak, R.S., 2001. A voxel-based morphometric study of ageing in 465 normal adult human brains. NeuroImage 14 (1 Pt 1), 21–36.

Green, M.A., Bilston, L.E., Sinkus, R., 2008. In vivo brain viscoelastic properties measured by magnetic resonance elastography. NMR Biomed. 21, 755–764.

Hamhaber, U., Sack, I., Papazoglou, S., Rump, J., Klatt, D., Braun, J., 2007. Three-dimensional analysis of shear wave propagation observed by in vivo magnetic resonance elastography of the brain. Acta Biomater. 3 (1), 127–137.

Hrapko, M., van Dommelen, J.A.W., Peters, G.W.M., Wismans, J.S.H.M., 2008. The influence of test conditions on characterization of the mechanical properties of brain tissue. J. Biomech. Eng. 130, 0310010–0310031.

Hsu, J.L., Leemans, A., Bai, C.H., Lee, C.H., Tsai, Y.F., Chiu, H.C., Chen, W.H., 2008. Gender differences and age-related white matter changes of the human brain: a diffusion tensor imaging study. NeuroImage 39 (2), 566–577.

Klatt, D., Hamhaber, U., Asbach, P., Braun, J., Sack, I., 2007. Noninvasive assessment of the rheological behavior of human internal organs using multifrequency MR elastography: a study of brain and liver viscoelasticity. Phys. Med. Biol. 52 (24), 7281–7294.

Klatt, D., Asbach, P., Somasundaram, R., Hamm, B., Braun, J., Sack, I., 2008. Assessment of the solid–liquid behavior of the liver for the diagnosis of diffuse disease using magnetic resonance elastography. Röfo 180, 1106–1109.

Koeller, R.C., 1984. Applications of fractional calculus to the theory of viscoelasticity. J. Appl. Mech. 51 (2), 299–307.

Kruse, S.A., Rose, G.H., Glaser, K.J., Manduca, A., Felmlee, J.P., Jack Jr., C.R., Ehman, R.L., 2008. Magnetic resonance elastography of the brain. NeuroImage 39 (1), 231–237.

Lu, Y.B., Franze, K., Seifert, G., Steinhauser, C., Kirchhoff, F., Wolburg, H., Guck, J., Janmey, P., Wei, E.Q., Kas, J., Reichenbach, A., 2006. Viscoelastic properties of individual glial cells and neurons in the CNS. Proc. Natl. Acad. Sci. U. S. A. 103 (47), 17759–17764.

McCracken, P.J., Manduca, A., Felmlee, J., Ehman, R.L., 2005. Mechanical transient-based magnetic resonance elastography. Magn. Reson. Med. 53 (3), 628–639.

Morrison, J.H., Hof, P.R., 1997. Life and death of neurons in the aging brain. Science 278 (5337), 412–419.

Mueller, S.G., Schuff, N., Weiner, M.W., 2006. Evaluation of treatment effects in Alzheimer's and other neurodegenerative diseases by MRI and MRS. NMR. Biomed. 19 (6), 655–668.

Pakkenberg, B., Pelvig, D., Marner, L., Bundgaard, M.J., Gundersen, H.J., Nyengaard, J.R., Regeur, L., 2003. Aging and the human neocortex. Exp. Gerontol. 38 (1–2), 95–99.

Papazoglou, S., Hamhaber, U., Braun, J., Sack, I., 2007. Horizontal shear wave scattering from a nonwelded interface observed by magnetic resonance elastography. Phys. Med. Biol. 52 (3), 675–684.

Papazoglou, S., Hamhaber, U., Braun, J., Sack, I., 2008. Algebraic Helmholtz inversion in planar magnetic resonance elastography. Phys. Med. Biol. 53 (12), 3147–3158.

Pelvig, D.P., Pakkenberg, H., Stark, A.K., Pakkenberg, B., 2007. Neocortical glial cell numbers in human brains. Neurobiol Aging.

Sack, I., Beierbach, B., Hamhaber, U., Klatt, D., Braun, J., 2008. Non-invasive measurement of brain viscoelasticity using magnetic resonance elastography. NMR. Biomed. 21 (3), 265–271.

Sinkus, R., Siegmann, K., Xydeas, T., Tanter, M., Claussen, C., Fink, M.M.R., 2007. elastography of breast lesions: understanding the solid/liquid duality can improve the specificity of contrast-enhanced MR mammography. Magn. Reson. Med. 58 (6), 1135–1144.

Terry, R.D., DeTeresa, R., Hansen, L.A., 1987. Neocortical cell counts in normal human adult aging. Ann. Neurol. 21 (6), 530–539.

Thibault, K.L., Margulies, S.S., 1998. Age-dependent material properties of the porcine cerebrum: effect on pediatric inertial head injury criteria. J. Biomech. 31, 1119–1126.

Tschoegl, N.W., 1989. The Phenomenological Theory of Linear Viscoelastic Behavior. Springer, Berlin.

Van Essen, D.C., 1997. A tension-based theory of morphogenesis and compact wiring in the central nervous system. Nature 385 (6614), 313–318.

Vappou, J., Breton, E., Choquet, P., Goetz, C., Willinger, R., Constantinesco, A., 2007. Magnetic resonance elastography compared with rotational rheometry for in vitro brain tissue viscoelasticity measurement. Magma 20 (5–6), 273–278.

Wuerfel, J., Beierbach, B., Klatt, D., Papazoglou, S., Hamhaber, U., Braun, J., Sack, I.M.R., 2008. elastography reveals tissue degeneration in Multiple Sclerosis patients. In: Proceedings 16th Scientific Meeting, International Society for Magnetic Resonance in Medicine. Toronto 1547.

Xu, L., Lin, Y., Han, J.C., Xi, Z.N., Shen, H., Gao, P.Y., 2007. Magnetic resonance elastography of brain tumors: preliminary results. Acta Radiol. 48 (3), 327–330.